

Article

Development of a Solid Catalyst Based on Pt Supported on Heterostructure (NaNbO₃/NaNb₃O₈/NiO) Applied to the Photodegradation of Phenol in Seawater

Kimberly G. Costa and Yvan J. O. Asencios * 

Institute of Marine Sciences, Federal University of São Paulo (UNIFESP), R. Maria Máximo 168, Santos 11030-100, SP, Brazil

* Correspondence: yvan.jesus@unifesp.br

Abstract: Phenol and its derivatives are present in effluents from several industrial processes, such as petroleum refining (produced water) and the pharmaceutical industry, and they are highly toxic. The present work elaborated a new catalyst for the removal of phenol and its derivatives. The photocatalyst was prepared by a simple method from the ammonium oxalate of niobium and nickel nitrate, resulting in heterostructures (principally NaNbO₃/NaNb₃O₈ and a lesser amount of NiO) named NiNb. Platinum was deposited on this catalyst (NiNb/Pt catalyst), and its photocatalytic activity was tested on the degradation of phenol in seawater and distilled water, in the presence and absence of UV-C light (germicidal, $\lambda = 254$ nm), and with varying concentrations of platinum and varying pH of the solution. The catalyst was characterized by different techniques (SEM, EDS, DRS, XRD, TXRF, S_{BET}). The results of the study showed that the NiNb/Pt catalyst achieved 65% phenol removal in seawater and about 57% removal in distilled water. The reuse of the catalyst was also studied, and the photocatalytic mechanism was investigated by tests with scavenger agents and terephthalic acid.

Keywords: niobates; platinum; seawater; photocatalysis; phenol



Citation: Costa, K.G.; Asencios, Y.J.O.

Development of a Solid Catalyst Based on Pt Supported on Heterostructure (NaNbO₃/NaNb₃O₈/NiO) Applied to the Photodegradation of Phenol in Seawater. *Catalysts* **2022**, *12*, 1565. <https://doi.org/10.3390/catal12121565>

Academic Editors: Krzysztof Miecznikowski and Beata Krasnodębska-Ostrega

Received: 10 September 2022

Accepted: 21 November 2022

Published: 2 December 2022

Publisher's Note: MDPI stays neutral with regard to jurisdictional claims in published maps and institutional affiliations.



Copyright: © 2022 by the authors. Licensee MDPI, Basel, Switzerland. This article is an open access article distributed under the terms and conditions of the Creative Commons Attribution (CC BY) license (<https://creativecommons.org/licenses/by/4.0/>).

1. Introduction

Phenol and its derivatives are toxic and persistent in the environment; even at low concentrations, they can impact water resources, affecting human health and all marine fauna and flora [1]. Such pollutants can reach the ocean through produced water, which is characterized as a byproduct of oil and gas production, arising from the extraction process, and it can be used for reinjection, reuse, or disposal [2,3]. According to the report of the Brazilian National Agency for Petroleum, Natural Gas, and Biofuels in November 2021, the estimated amount of produced water was 2.852 million barrels per day [4].

Produced water is composed of benzene, toluene, ethylbenzene and xylene (BTEX), naphthalene, phenanthrene, dibenzothiophene (DBT), polyaromatic hydrocarbons (PAH), phenols, gases (H₂S, CO₂, and O₂), and heavy metals (As, Ba, Cd, Cr, Cu, Fe, Pb, Mn, Hg, Mo, Ni, V, Zn) [3,5,6]. Produced water also has the same constituents as seawater, but at different concentrations, inorganic ions such as Na⁺, Cl⁻, Ca²⁺, Sr²⁺, Mg²⁺, and K⁺ are present [3]. Considering the composition of the produced water, a phenol solution in seawater was chosen as a simulated effluent. Phenol was chosen because it has a high solubility in seawater, is a toxic compound to the environment, and is present in effluents from petroleum refining. Furthermore, phenol has been used in studies that aim to simulate the fraction of aromatic compounds in water produced from petroleum [7–10].

On the other hand, seawater was used considering its high content of salts, which is similar to that found in produced water [3]. In addition, in longer times of extraction of the reservoirs, seawater can predominate in the composition of produced water, since seawater is used as an injection fluid in the reservoir.

In some cases, produced water needs to be dumped. However, before this, it must meet environmental standards, such as those of the CONAMA (The National Environment Council of Brazil) resolution 430/11, which determines, among other pollutants, that total phenol emissions must not exceed $0.5 \text{ mg}\cdot\text{L}^{-1}$ [11]. With increasingly restrictive legislation, the search for efficient and viable technologies for the treatment of produced water is essential. An alternative to addressing this problem is heterogeneous photocatalysis; previous studies have demonstrated its efficiency [12–15]. This process uses a solid catalyst (a semiconductor) that when activated by UV-light generates highly oxidizing radicals, such as $\bullet\text{OH}$ [16], that are capable of oxidizing organic molecules present in the aqueous medium, leading to total mineralization ($\text{CO}_2 + \text{H}_2\text{O}$).

Niobium and its oxides have been explored as catalysts quite efficiently, but studies with niobates are recent and more focused on hydrogen production and the photodegradation of synthetic dyes in distilled water. For example, Yang et al. [17] synthesized a Pt/N-rGO/N-NaNbO₃ through the hydrothermal method, obtaining a hydrogen production equivalent to $2342 \text{ }\mu\text{mol}\cdot\text{g}^{-1}\cdot\text{h}^{-1}$.

The term “heterostructure” refers to a combination of two semiconductors, which must differ in their band gap, lattice parameter, stoichiometry, and chemical nature with varying degrees of complexity [18]. The advantage of working with heterostructures is the inhibition of electronic recombinations, which improves photocatalytic activity [19]. The use of heterostructures in photocatalysis was demonstrated previously by Li et al. [20], who applied AgSbO₃/NaNbO₃ in the photodegradation of Rhodamine B (RhB) dye, as well as Kumar et al. [21] who applied a CdS/NaNbO₃ to remove methylene blue (MB); among other researchers. On the other hand, Nickel oxide (NiO) is a well-known semiconductor material (p-type), with a wide band gap, and good chemical and thermal stability, it has applications in catalysis, photocatalysis, and the manufacture of cathodic batteries, gas sensors, electrochromic films, fiber optics, and solar cells [15,22,23].

In the present paper, a simple synthesis method to obtain a heterostructured material is described. The synthesized heterostructure is composed of two sodium niobates (NaNbO₃/NaNb₃O₈) and nickel oxide (NiO), and the photocatalytic properties of this material were evaluated.

Few works have focused on the application of heterogeneous photocatalysis in effluents with high salinity, reinforcing the importance of further research on this issue. Silva et al. [24] demonstrated the application of Heterogeneous-Photocatalysis and Photo-Fenton (using TiO₂ and FeSO₄·7H₂O as catalysts, respectively), to treat two types of effluents: a model solution of phenol in seawater and a real sample of oil-produced water. Their results showed a maximum of 99% of phenol removal, despite the high content of salts present in seawater. Wang et al. [25] applied a catalyst of SiO₂-TiO₂ doped with La³⁺ and used graphene oxide for the treatment of a phenol solution in seawater ($15 \text{ mg}\cdot\text{L}^{-1}$), obtaining 90% removal.

Performing Heterogeneous-Photocatalysis in seawater is a big challenge because of its high salinity. Therefore, in the present work, aiming to improve the photocatalytic activity of the catalysts, a noble metal (Pt) was used, as it is known that the deposition of noble metals on the surface of a semiconductor forms a Schottky barrier, which can optimize the photocatalytic process [23].

In a simple search on the Web of Science, using the keyword ‘sodium niobate’ (and filtering by nickel oxide), only five results appear in return, and none of these address the application in heterogeneous photocatalysis. George et al. [26,27] synthesized a mixture of NaNbO₃/NiO as a dielectric material. The synthesis of such a material involved two calcination steps, one at 699 °C and the second step at 1039 °C. Zielińska et al. [28] and Iwase et al. [29] synthesized sodium niobate and nickel oxide (NiO/NaNbO₃) catalysts and applied them to hydrogen production. In the material synthesized by both authors, there were two calcination steps, the first occurring in 11 h. In their work, Kioka et al. [30] discuss the obtainment of nanostructures for the manufacture of transparent materials that can be used as fiber optic glasses, through the formation of NaNbO₃ from the crystallization

of glass composed of $30 \text{ Na}_2\text{O} - 25 \text{ Nb}_2\text{O}_5 - (45 - x) \text{ SiO}_2 - x \text{ AlO}_{1.5}$. The nickel oxide added to an improvement of the laser adsorption in the optical fiber; this material because is made of glass components and thus demands high calcination temperatures ($1500 \text{ }^\circ\text{C}$).

In comparison to reports mentioned above that also study niobates, the synthesis method described in our paper proved to be quite simple because it occurs in a single step (by coprecipitation of the precursors) and needs only one calcination step (at $500 \text{ }^\circ\text{C}$). In this way, it is important to comment that such characteristics follow some of the Green Chemistry Principles, in aspects such as the prevention of waste, being free of solvents, and less energy consumption [31].

Finally, the objective of the present work was to degrade phenol in seawater by heterogeneous photocatalysis under UV-C radiation (254 nm), using catalysts based on a heterostructure material (of Ni, Nb, O, and Na) promoted by platinum.

2. Results and Discussions

2.1. Catalyst Characterization

2.1.1. X-ray Diffraction (XRD) Analysis

The crystallographic pattern of the synthesized material (the NiNb catalyst) is shown in Figure 1. According to the XRD result, the NiNb catalyst consists of a mixture formed by a heterostructure of sodium niobate ($\text{NaNbO}_3/\text{NaNb}_3\text{O}_8$) and nickel oxide (NiO). According to the ICDD database, the peaks of the XRD pattern of the catalyst correspond to PDF N° 21-1367, 74-2436, and 73-1519, demonstrating the orthorhombic crystalline phase of niobates [32]. These results indicate that sodium niobates are present in the forms of NaNbO_3 and NaNb_3O_8 , corroborating the formation of the heterostructure. Furthermore, the occurrence of irregular peaks of low intensities at Bragg angles that correspond to PDF N° 73-1519 indicates the presence (in minor proportion) of nickel oxide (NiO) in FCC (face centered cubic) structure.

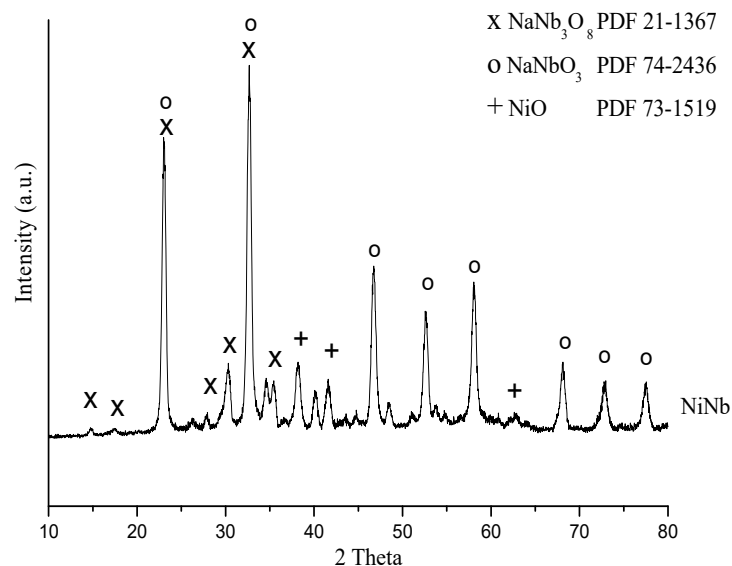


Figure 1. Results of X-ray diffraction (XRD) analysis of the NiNb catalyst.

2.1.2. Diffuse Reflectance Spectroscopy (DRS) Analysis

Generally, the catalysts used in the photocatalytic degradation of organic contaminants and the photocatalytic production of hydrogen from water are semiconductor materials, such as transition metal oxides, e.g., ZnO , ZnS , Fe_2O_3 , CdS , and TiO_2 , among others. Most of these compounds are activated by UV radiation ($<350 \text{ nm}$ or a band gap energy $>3.0 \text{ eV}$) [33,34]. However, these compounds have a band gap in the range of 3.0 to 3.2 eV , which prevents the use of visible light (which accounts for most of the solar energy). Therefore, in this work, UV-C radiation was used to activate the NiNb catalyst.

The DRS spectrum of the catalyst after treatment by the Kubelka–Munk function $f(R)$ is shown in Figure 2. The arrow indicates the tangent line to the curve, which, when reaching the X-axis, indicates the band gap energy of the NiNb catalyst [35].

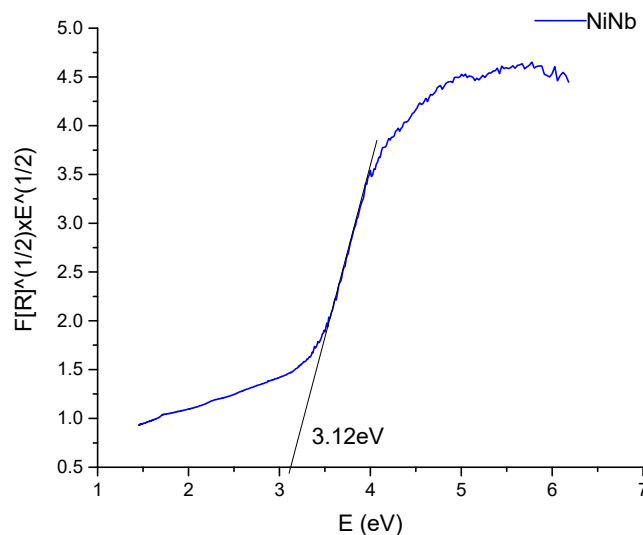


Figure 2. Result of Diffuse Reflectance Spectroscopy (DRS) analysis of the NiNb catalyst.

Figure 2 demonstrates that the NiNb catalyst has a band gap of approximately 3.12 eV. This band gap is close to the band gap of lamellar potassium niobates (KNb_3O_8 and $\text{K}_4\text{Nb}_6\text{O}_{17}$), whose energy is 3.65 eV and 3.62 eV, respectively [36]. Praxedes [37], in his work with sodium niobates and potassium niobates, he found a band gap equivalent to 3.49 eV for NaNbO_3 and 3.27 eV for KNbO_3 . The NiNb catalyst also has a band gap similar to TiO_2 , which is 3.2 eV [38], the latter being the most used catalyst in photocatalysis.

2.1.3. Surface Area (S_{BET}), Particle Size Distribution, and Zeta Potential

Figure 3 shows the particle size distribution of the NiNb catalyst. This figure reveals the presence of only one peak with a size between 900 and 1800 nm, indicating dispersed particles with almost no agglomeration (a narrow distribution of the particle size). Adsorption of nitrogen measurement (S_{BET}) indicated a surface area of $5.030 \text{ m}^2 \cdot \text{g}^{-1}$, this small surface area can be considered as a result of the large particle of this catalyst [39], observed in the particle size distribution. According to the zeta potential measurement, the surface charge of NiNb is -38.20 mV (at the natural pH of the solution), the value is close to that found by Ghorai and Dhak [40] for a catalyst composed of niobium and titanium oxides with a surface charge of -24 mV . According to this analysis, at natural pH the NiNb catalyst has negatively charged particles on the surface, this property can influence the adsorption of molecules on the catalyst surface during photocatalysis.

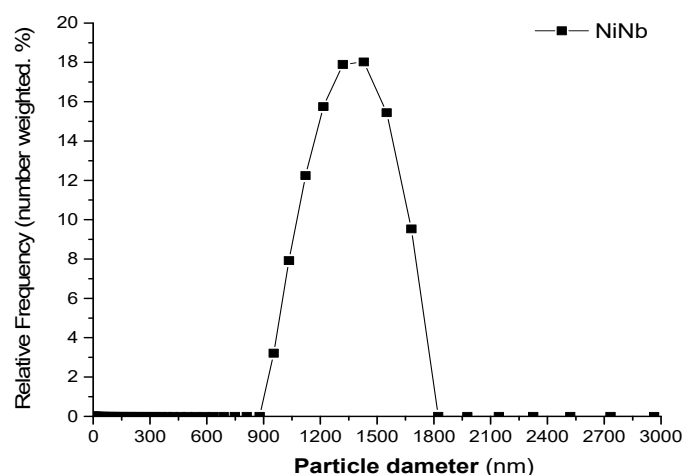


Figure 3. Particle size distribution and surface charge.

2.1.4. Scanning Electron Microscope (SEM) Analysis

The SEM analysis shows that the NiNb catalyst has a morphology in the form of small, smooth, and homogeneous agglomerates, as illustrated in Figure 4. Materials with similar morphology were found by Assis [41] who synthesized NaNbO_3 , and by Wu and Xue [42] who synthesized NaNb_3O_8 .

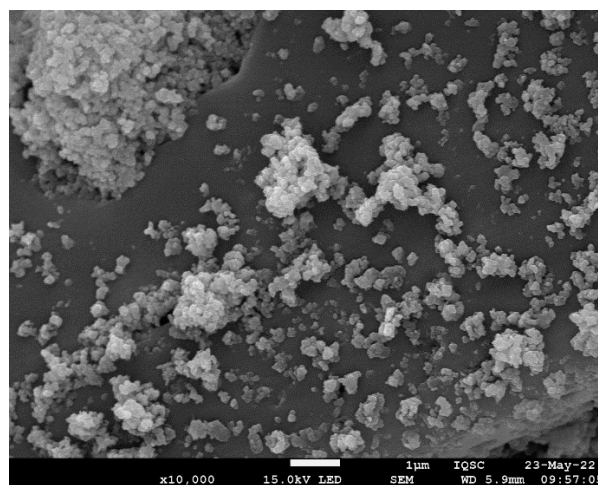


Figure 4. Image obtained by Scanning Electron Microscopy (SEM) of the NiNb catalyst ($\times 10,000$ approximations).

2.1.5. Total Reflection X-ray Fluorescence (TXRF) Analysis

The TXRF results of the catalysts (the NiNb catalyst, and the same catalyst after Pt deposition: NiNb/Pt) are shown in Table 1, the composition of the samples is expressed in weight percent (wt, %). According to this table, the NiNb catalyst is composed principally of nickel and niobium, with a purity of 99.97%, and 0.03% of impurities corresponding to the reagents used for the synthesis of this catalyst. In the NiNb/Pt catalyst, in addition to nickel and niobium, the presence of platinum was also detected, but in a smaller amount than expected, which suggests that the deposition method of this metal on the catalysts was not very effective (probably there was a loss of platinum during the deposition procedure). Another possibility is the leaching of a small quantity of the platinum after the photocatalytic test, as the NiNb/Pt catalyst for this analysis was that one recovered after the first cycle of photocatalysis (see the methodology). As the NiNb/Pt catalyst was that recovered after one cycle of use, other compounds from seawater such as Cl, K, P, Cr, and S were present in the sample, the latter being from sulfate anions [3] (Table 1).

Table 1. Results obtained from the TXRF analysis of the catalysts (average values).

Element	Weight %	
	NiNb	NiNb/Pt
P	–	0.0137
S	–	3.6281
Cl	–	40.0911
K	0.011	0.8279
Ca	0.0091	1.4181
Ti	0.0017	0.0037
Fe	0.0026	0.0046
Cr	–	0.023
Ni	1.8689	0.762
Cu	0.0049	–
Zn	0.0023	0.0022
Nb	98.099	53.0232
Nd	0.0004	–
Pt	–	0.2023

According to Section 2.1.1, the XRD analysis indicates the presence of (NaNbO₃/NaNb₃O₈) heterostructure, therefore, sodium (Na) is expected in the catalyst composition in the TXRF analysis, however, it wasn't detected owing to the limitation of this technique. TXRF can identify elements with an atomic number equal to/or higher than 12, since sodium is an element of low atomic number (Z = 11) it was not possible to quantify it by TXRF.

2.1.6. Energy Dispersive X-ray Analysis (EDX)

For a better understanding of the composition of the catalyst, in special for the quantification of sodium, the NiNb catalyst was analyzed by Energy Dispersive X-Ray Analysis (EDX), and the results are shown in Table 2. The results confirmed the presence of the elements expected for the NiNb heterostructure (NaNbO₃/NaNb₃O₈ and NiO), detailed in Section 2.1.1.

Table 2. Chemical composition of NiNb catalyst obtained by EDX (average values, weight percent, %wt).

Element	NiNb
	wt %
O	47.87
Na	23.99
Ni	3.32
Nb	24.82

2.2. Photocatalytic Tests

Unless it is mentioned, all the photocatalytic tests were carried out with the phenol solution made in seawater. Figure 5 presents a comparative study of the phenol removal (%) in seawater. This figure shows the results obtained in the test in the dark (that is in the absence of UV-light but with the catalyst), using a ratio of 0.0125 g of catalyst to 25 mL of phenol solution. The figure also contains the result of the photocatalytic test in the presence of UV-light but without catalyst (blank test), and the results of the photocatalytic test in the

presence of UV-light and catalyst. Each test has a specific objective: the test carried out in the dark, with the catalyst, aims to verify the contribution of the adsorption of phenol on the surface of the photocatalyst, whereas the blank test, in the presence of UV light (without catalyst), was used to evaluate the photodegradation of phenol, only by photolysis.

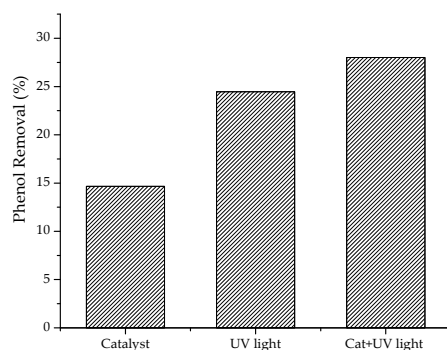


Figure 5. Comparative tests of adsorption (in dark, 0.0125 g of the NiNb catalyst, 25 mL of phenol solution in seawater, and pH = 3.5), photolysis (only UV-light for 1 h, without catalyst, 25 mL of phenol solution in seawater, and pH = 3.5), and heterogeneous-photocatalysis (0.0125 g of the NiNb catalyst + UV light for 1 h, 25 mL of phenol solution in seawater, and pH = 3.5).

According to Figure 5, in the presence of the NiNb catalyst but without UV irradiation (dark test), the phenol removal % is very low. This suggests that the adsorption of phenol on the catalyst is not favored. This might be due to the low surface area of the catalyst ($5.030 \text{ m}^2/\text{g}$), when compared for example to TiO_2 [43]. Gonçalves et al. [44] reported in their study that a commercial Nb_2O_5 has a specific surface area of $1.50 \text{ m}^2/\text{g}$, which can increase to $2.40 \text{ m}^2/\text{g}$ if calcined at $600 \text{ }^\circ\text{C}$. Figure 5 also shows a higher percentage of removal in the blank sample, which indicates that photolysis is favored more than the adsorption process.

However, according to Figure 5, the combination of UV-light and the NiNb catalyst increased the phenol removal %, demonstrating that heterogeneous photocatalysis took place. It is well-established [12–15] that when solid semiconductors (which have valence bands (VB) and conduction bands (CB), separated by a gap of energy- also known as band gap energy), are irradiated with photons with energy higher than the band-gap energy of the material, electrons from the valence band are promoted to the conduction band. This process forms electron–holes (h^+) in the valence band. These electron–holes (h^+) are capable to oxidize organic molecules in water, they can also break water molecules and generate hydroxyl radicals ($\bullet\text{OH}$), and through these radicals trigger the oxidation of contaminants present in water [16].

To increase the phenol removal % obtained by the NiNb catalyst in heterogeneous photocatalysis, this catalyst was impregnated with Platinum. As will be described in the methods, the amount of Pt (added as hexachloroplatinic acid solution, and impregnated by photodeposition method) was varied as 100, 500, and 1000 μL , which correspond to 0.32%, 1.6%, and 3.2% Pt. Figure 6 shows the results of phenol removal % obtained in the heterogeneous photocatalysis using the NiNb catalyst with various platinum concentrations, as well as the kinetic study.

The presence of noble metals (in this case, Pt) on the surface of a semiconductor generates a phenomenon known as the Schottky barrier [23]. This process consists of decreasing the work function of the semiconductor and increasing that of the metal until the energy levels are equal. In this way, both obtain negative and positive charges in excess, forming a barrier capable of capturing photogenerated electrons (e^-_{CB}) on the semiconductor surface and suppressing the recombination of electron-hole pairs, thus increasing the photocatalytic activity of the semiconductor [23].

As shown in Figure 6, a higher amount of platinum (1000 μL) added to the catalyst increased the phenol removal up to 65%. In this test, it was possible to verify that the

reaction reached the equilibrium after 5 h. During the tests, it was verified that the catalyst does not change the salinity of the water, that is, it cannot remove the mineral salts present in the seawater, because the salinity remained the same (approximately 30 ppm) before and after the photocatalytic test.

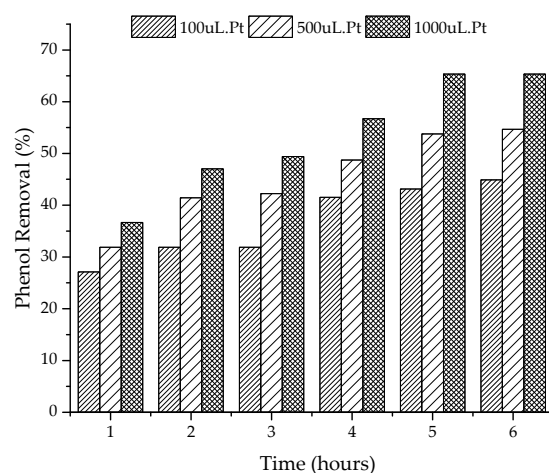


Figure 6. Kinetics of heterogeneous photocatalysis reaction in seawater with 0.0125 g of catalyst, 1 to 6 h of UV light, an amount of platinum (100, 500, or 1000 μ L), and pH = 3.5.

Figure 7 presents the results of phenol removal (%) obtained by heterogeneous photocatalysis under the same conditions as the test presented in Figure 6, however, this time the tests were carried out with a phenol solution made in distilled water (aiming to see the effect of salts in the photocatalytic process). Figure 7 shows that equilibrium was reached in 5 h with 55% removal. Thus it is very clear that the phenol removal % in distilled water is lower than that shown for seawater (see Figure 6).

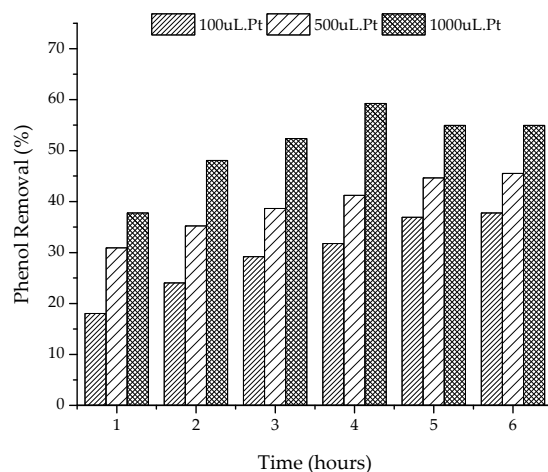


Figure 7. Kinetics of heterogeneous photocatalysis reaction in distilled water with 0.0125 g of catalyst, 1 to 6 h of UV light, an amount of platinum solution (100, 500, or 1000 μ L), and pH = 3.5.

The present study demonstrated that the NiNb/Pt catalyst presents a superior performance in seawater. Thus, it is possible to infer that the salts present: Na^+ , K^+ , Ca^{2+} , Mg^{2+} , and Cl^- might have contributed to the increase of the ionization of phenol molecules, making them more soluble in water, as it is known that phenolic compounds can coordinate with the metallic cations present in water [45,46]. Furthermore, such salts may also contribute to the diffusion of phenol molecules in the pores of the catalyst, all these characteristics could be favoring the photocatalytic performance in seawater. The catalyst

demonstrated the ability to overcome interactions generated by salts such as K^+ , Ca^{2+} , Cl^- , Na^+ , and Mg^{2+} , which could compete with the oxidizing centers of phenol, making an inhibitory effect during the photodegradation process, but it seems that this effect did not occur, since these salts are in their maximum oxidation state [12,47,48].

Other authors have also demonstrated better results in removing contaminants from saline effluents than from distilled water [25,49,50]. For example, Iguchi et al. [51] improved the phototacalytic reduction of CO_2 through the addition of 0.1 M NaCl.

The interaction of phenol molecules with seawater salts can lead to the formation of derivated phenolic compounds, such as chlorophenols, which can be formed from chloride ions under UV irradiation [52]. The colorimetric method used in our research [45,46] quantifies the total phenolic compounds, so it is possible to deduce that such derivated compounds were also removed during the photocatalytic process.

2.2.1. Variation of pH of the Phenolic Solution

The phenol removal by heterogeneous-photocatalysis using NiNb/Pt catalyst were studied under different pH of the initial solution, the results are shown in Figure 8. As shown in Figure 8, the best results of phenol removal % were at pH 1.0, 3.5, 7.0, and 8.5. The test carried out at pH 10 recorded the worst result.

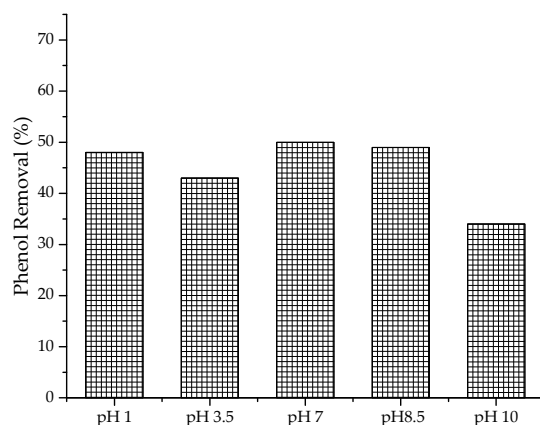


Figure 8. Phenol removal after 5 h of UV irradiation, at different pH of the initial phenolic solution (0.0125 g of catalyst, 500 μ L of platinum solution).

The adsorption of phenol on the surface of the catalyst is favored when it is in undissociated form, this occurs at low pH. This can explain the better performance in removing phenol at pH below 8.5, and at acidic pH. Previous works have shown that in heterogeneous photocatalysis, phenol is better removed at pH 3 [16,24]. Thus, based on experimental data from other studies, this project was chosen to work with a pH in the range of 3.0 to 3.5.

The results obtained at pH 7 can be explained by the increase of phenol solubility and the abundance of hydroxyl ions, preventing the diffusion of phenolic ions [53].

In this study, the natural pH of the model effluent is pH is 8.4 (phenolic solution without pH modification), and after the addition of the NiNb/Pt catalyst the pH rises to 8.5. The removal of phenol % achieved at this pH is similar to that obtained at pH 7.

At pH above 9, phenol is converted to negatively charged phenoxide, thus decreasing the adsorption capacity, as the photocatalyst surface is negatively charged, this can cause a repulsive force against the phenolate ion [16,24,53].

The pH of the oil-produced water can vary between 4.3 and 10.0 [3]. In our study, the pH 3.5 for the phenol solution was chosen based on previous studies, as niobium compounds are normally used in acid catalysis [16,24,54]. However, in the study of the variation of pH of the solution, it is possible to see that the catalyst can perform very well at a wide range of pH, from pH 1.0 to 8.5. Applying the catalyst without pH correction

(pH 8.5) would be very interesting for further studies since CONAMA resolution 430/11 establishes that effluents must be disposed of in a pH range between 5.0 and 9.0 [11].

2.2.2. Oxidizing Species

To verify the presence of active species generated during the photocatalytic process, scavengers of superoxide radicals ($O_2^{\bullet-}$), positively charged holes (h^+), and hydroxyl radicals ($\bullet OH$) were used. In these tests, the NiNb/Pt catalyst was used, under the same conditions previously established (5 h UV-irradiation, 500 μL of platinum solution, 25 mL of phenolic solution, and 0.0125 g of catalyst), however this time the scavenger agents (ethanol, p-benzoquinone, and KI) were present, and used separately, in order to extinguish a specific oxidizing species. Ethanol (EtOH), p-benzoquinone (BQ), and potassium iodide (KI) were added to capture the $\bullet OH$ radical, the anionic superoxide radicals ($O_2^{\bullet-}$), and the positively charged holes (h^+), respectively. [55,56]

Each test was compared with a blank sample, that is, the test without the scavenger agents. These results are shown in Figure 9, they are expressed in reduction percent (%), which means the reduction of phenol removal caused by the addition of such a scavenger. Only the photocatalysis process was considered for this account. In Figure 9, it is possible to observe that ethanol reduced the removal of phenol to approximately 25%, thus confirming the presence of $\bullet OH$ radicals in the photocatalytic reaction.

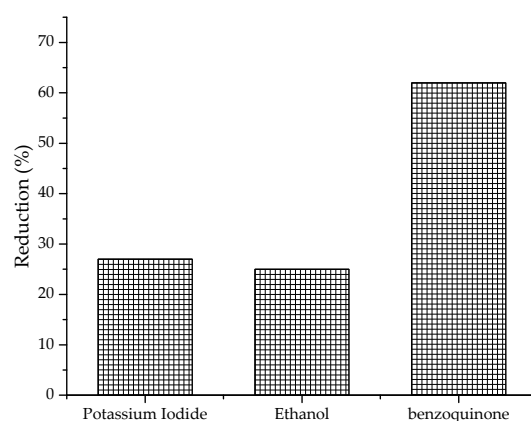


Figure 9. The effect of active species (2 mM of KI, ethanol and p-benzoquinone) on the photocatalytic reaction at 4 h of UV irradiation, 0.0125 g of catalyst, and 500 μL of platinum.

The reduction of 27% of the phenol removal caused by the addition of potassium iodide (KI) confirmed the presence of photogenerated vacancies (h^+_{VB}) in the photocatalytic reaction.

The presence of p-benzoquinone reduced the phenol removal to 62%, confirming that during the photocatalytic degradation of phenol, superoxide radicals ($O_2^{\bullet-}$) were produced. As this is the highest value of reduction, it can be affirmed that these radicals have more influence in the photocatalytic process occurring over NiNb/Pt [49]. Thus, it is possible to suggest that the decreasing order of influence of radicals on the phenol removal over NiNb/Pt is $O_2^{\bullet-} > h^+_{VB} > \bullet OH$.

2.2.3. Hydroxyl Radical ($\bullet OH$) Detection Experiments

For a better understanding of the presence of the hydroxyl radicals ($\bullet OH$) during the photocatalytic process, terephthalic acid (TA) was used as detailed in the methods. The reaction between the hydroxyl radicals and terephthalic acid (TA) produces 2-hydroxyterephthalic acid (2-HTA), as shown in Equation (1) [57,58]:



The formed compound (2-HTA) can be detected by fluorescence at a wavelength of 425 nm. The emission spectra fluorescent obtained from the photoreaction on NiNb and

NiNb/Pt catalysts are shown in Figure 10. It can be seen that the emission spectra fluorescent has an intense peak at 425 nm that corresponds to 2-HTA [57,58], thus confirming that only the NiNb/Pt catalyst promotes the formation of $\bullet\text{OH}$ radicals. These results are in agreement with those obtained in the photocatalytic tests, in which the presence of the Pt° significantly increased the photocatalytic performance of the NiNb catalyst.

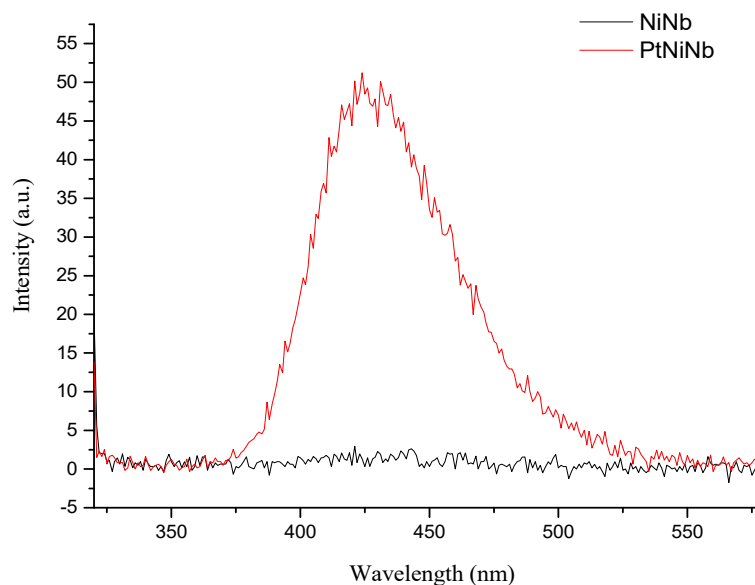


Figure 10. Fluorescence spectrum of 2-HTA after the photocatalysis. Black line shows the result obtained using the NiNb catalyst (0.0125 g), and red line shows the result obtained using the NiNb/Pt catalyst (0.0125 g of NiNb + 1000 μL of platinum in distilled water).

2.2.4. Proposed Mechanism

Due to the complex composition of seawater, the mechanism of heterogeneous photocatalysis in seawater is still unclear. However, based on other works [16,24,47] and taking into account the previous paragraphs in Sections 2.2.2 and 2.2.3 concerning oxidizing species, it is possible to infer the involved steps. The photodegradation of phenol occurs in three steps: the adsorption of phenol or water molecules on the surface of the photocatalyst, followed by photodegradation of the phenol surface, and the desorption of products from the surface of the photocatalyst.

As reported by refs. [16,24,47,59], during the photoactivation of the semiconductor catalyst, the valence band electrons (e^-_{VB}) are promoted to the conduction band (e^-_{CB}), generating electron vacancies in the valence band (h^+_{VB}), as illustrated in Equation (2):



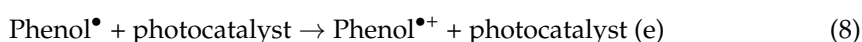
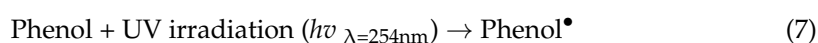
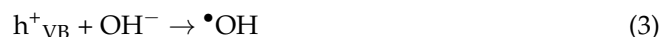
In the photodegradation mechanism, the predominant step is adsorption, either of the phenol molecules or the water molecules. In this step, the charge transfer from the semiconductor to the molecules adsorbed at the active points of the photocatalyst occurs, causing several redox reactions from active species such as vacancies generated by photons (h^+_{VB}), photo-promoted electrons (e^-_{CB}), hydroxyl radicals ($\bullet\text{OH}$), and superoxide ions ($\text{O}_2^{\bullet-}$), such reactions are favored by thermodynamic factors [60,61]. During irradiation, photochemical species of peroxides ($\text{O}_2^{\bullet-}$ radical superoxide) are generated from the presence of O_2 in the aqueous medium. Such a radical acts as a precursor of many reactive species, being an essential source of hydroxyl radical, also preventing the recombination of the electron-hole pair in the catalyst, thus improving the redox process [16,24,47,59].

The photodegradation mechanism can occur directly or indirectly. In the direct mechanism, the oxidative decomposition of the phenol molecules adsorbed on the surface of the photocatalyst occurs, whereby the species (h^+_{VB}), (e^-_{CB}), ($\bullet\text{OH}$), and ($\text{O}_2^{\bullet-}$) promote

the mineralization of the pollutant in CO_2 and H_2O . In the indirect mechanism, the H-O-H bonds of the adsorbed water molecules are broken, with the consequent generation of hydroxyl radicals, $\bullet\text{OH}$, which attack the phenol molecules in the reaction medium [47,59].

It is worth mentioning that among the redox reactions mentioned above, there is still the platinum photoreduction reaction, which also contributes to the oxidation of phenol molecules and its derivatives.

Yao et al. [59] proposed (in their work regards the immobilization of TiO_2 on activated carbon fiber) that the photodegradation of phenol follows the following reaction mechanism:



Based on the data obtained in Sections 2.2.1–2.2.3 and on the results of Figures 9 and 10, it is concluded that among the reactions (3–9), the reactions that are more favored in the photocatalytic process of our study are the reactions promoted by the superoxide radical ($\text{O}_2^{\bullet-}$) and by the $\bullet\text{OH}$ radical, seen in Equations (3)–(6) and (9). The abundance of these radicals in the reaction medium is due to the oxygen dissolved in water, due to the oxygen absorbed from the external environment (since the reactor is open to the air), and due to the dissociation of water molecules. The presence of these radicals in major proportion, together with the increase of the ionization of phenol (favored by the salts present in seawater), result in the good photocatalytic efficiency of the NiNb/Pt catalyst. Figure 11 presents an illustrative scheme of the dynamics of the proposed mechanism.

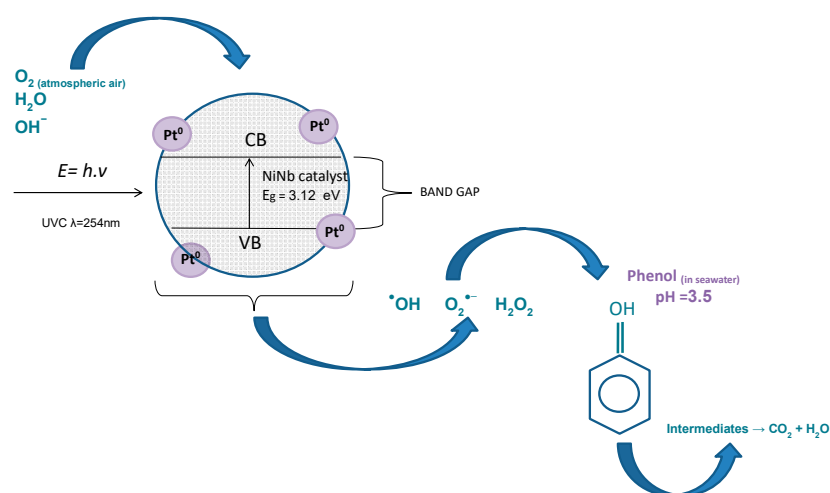


Figure 11. Scheme of the proposed mechanism (CB: conducting band; VB: valency band; E_g : band-gap energy). Source: prepared by the author.

2.2.5. Catalyst Reuse

According to Figure 12, in all samples, the photocatalyst reduced its removal capacity as the reuse cycles occurred. The decrease in the efficiency of the photocatalysts along the cycles was expected and may be related to the presence of salts in the seawater; these ions may be clogging the pores and active sites of the surface of the photocatalyst. The clogging of the pores by seawater salts is very possible because according to the TXRF analysis, a

high concentration of the element from seawater was detected, see Table 1 (NiNb/Pt). The decrease in efficiency can also be attributed to the leaching of a small part of Pt during the process of recovery of the catalyst after each cycle. There is a significant reduction in the phenol removal (%) after the first cycle, but the second and the third cycles remain almost constant, which suggests that the catalyst can remove phenol for further cycles and that can be reused. It also suggests that the platinum remained deposited in the catalyst. Table 1, presented previously, shows the composition of NiNb/Pt after one cycle.

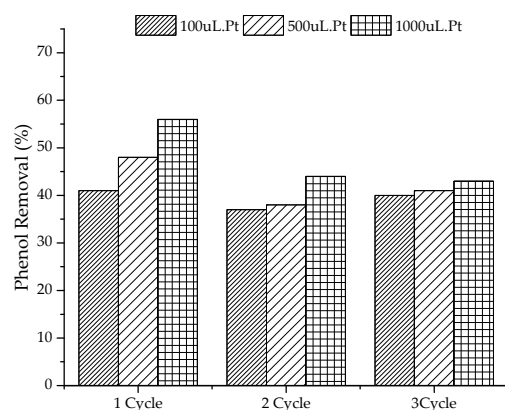


Figure 12. Result of photocatalyst reuse (every test lasted for 5 h under UV irradiation, 0.0125 g of catalyst, and an amount of platinum (100, 500, or 1000 µL)).

3. Materials and Methods

3.1. Catalyst Synthesis

10 g of ammonium niobium oxalate salt ($\text{NH}_4[\text{NbO}(\text{C}_2\text{O}_4)_2 \cdot \text{H}_2\text{O}] \cdot \text{XH}_2\text{O}$) (supplied by Brazilian Metallurgy and Mining Company, CBMM, Araxá, Brazil) and 1 g of nickel nitrate hexahydrate $\text{Ni}(\text{NO}_3)_2 \cdot 6\text{H}_2\text{O}$ (Sigma Aldrich, St. Louis, MO, USA), both dissolved in 100 mL of water, were precipitated at room conditions with 20 mL of NaOH solution (5 mol/L), resulting in a green-milky colloid. The pH of this former colloid was subsequently regulated to pH 8. This precipitate was then washed continuously to remove excess sodium, dried at 80 °C (for 12 h), and finally calcined at 500 °C (at a heating rate of 5 °C·min⁻¹) for 1 h in the presence of atmospheric air. This catalyst was named NiNb. The methodology was adapted from Carvalho et al. [62] and Nogueira et al. [63].

3.2. Catalyst Characterization

The crystalline phases were characterized by X-ray diffraction analysis (XRD) in a Rigaku Multiflex diffractometer (Rigaku Corporation, Tokyo, Japan) (30 kV, 10 mA), in the range $2\theta = 5\text{--}80^\circ$, using Cu-K α radiation ($\lambda = 1.5406 \text{ \AA}$). The identified diffraction data were compared with the International Center for Diffraction Data (ICDD) database. UV-visible diffuse reflectance spectroscopy (DRS) analysis of the photocatalyst was performed on a Varian Cary 100 Bio UV/VIS spectrophotometer (Varian Inc./Agilent Technologies, Ottawa, ON, Canada) equipped with integrating sphere diffuse reflectance along with BaSO_4 as a reference material. The measured reflectance data R were transformed with the Kubelka–Munk function $f(R)$ to determine the gap value through the Tauc plot. The energy of the band gap of the photocatalyst was determined according to the method of Woody and Tauc, 1972 [64]. The band gap of the photocatalyst was determined by linear extrapolation of the steep part of the DRS profile, towards the baseline. The gap energy (E_g) was estimated by the following formula (Tauc graph) [64]: $(\alpha h\nu)^n = A(h\nu - E_g)$, where α is the absorbance, $h\nu$ is the photon energy, “A” is related to the effective masses associated with the valence and conduction bands, and n is $n = 2$ for a permissible indirect transition or $n = 1/2$ for a direct transition.

Scanning electron microscopy (SEM) and energy-dispersive X-ray analysis (EDX) were performed in LEO equipment, model 440 (Shimadzu Corp., Kyoto, Japan), and JEOL JSM-

6700F (Japan) field emission with a secondary electron detector (SE) at an accelerating voltage of 20 kV.

To measure the surface area BET (S_{BET}), a Micromeritics FlowSorb II 2300 equipped with a Micromeritics AutoMate 23 (Shimadzu Corp., Japan) was used. The particle size and the zeta potential of the photocatalyst were obtained in a Zetasizer Nano ZS90 (Malvern, PA, USA).

The NiNb catalyst (before and after a photocatalytic cycle) was analyzed by Total Reflection X-ray Fluorescence (TXRF) in a S2 Picofox spectrometer (Bruker AXS Microanalysis GmbH, Berlin, Germany). The conditions for TXRF were: measurement time 300 s, voltage 40 kV, 50 W X-ray tube, molybdenum target, and silicon drift detector. In this analysis, the samples were prepared as follows: 50 mg of catalysts (powdered and dried) were added to 1 mL of 1% Triton, forming a homogeneous suspension, after that, 10 μL of gallium was added as an internal standard. The suspension was homogenized, and then 10 μL of this suspension was pipetted in the center of a quartz reflective support and dried in an oven at 60 °C. The samples were measured in duplicates. The TXRF spectra were analyzed by the software provided with the S2 Picofox spectrometer.

3.3. Photocatalytic Tests

All tests were performed in triplicate with a phenol solution (40 ppm) prepared with seawater as the solvent. The seawater was previously filtered through a membrane filter (0.2 μm) to remove suspended organic matter. Seawater was collected in a preserved region of Guarujá City (São Paulo, Brazil).

The photocatalytic tests were carried out in a dark chamber with internal ventilation and exhaust. For UV irradiation, six germicidal UV-C light tubular lamps (15 W G13, 254 nm, 220 volts) were used. The tests were carried out in a batch system using glass beakers (500 mL) as reactors and a continuous stirrer. The irradiation reached the solution directly from the top of the reactor. A phenol concentration of 40 ppm in seawater was used for every photocatalytic test; before the irradiation, the suspension (catalysts/phenol solution) was stirred in the dark for 20 min, and then the irradiation started with time variations from 1 to 6 h. For each catalytic test, 25 mL of phenol solution and 0.0125 g of catalyst were used, forming a suspension with a concentration of 0.5 $\text{g}_{\text{cat}} \cdot \text{L}^{-1}$.

In the tests, parameters such as degradation time, the influence of UV light, and the presence of platinum were verified.

Test of variation of platinum on the catalyst: The Pt^0 was deposited on the catalytic surface by the photodeposition of hexachloroplatinic acid ($\text{H}_2\text{Cl}_6\text{Pt} \cdot 6\text{H}_2\text{O}$) solution. The amount Pt of hexachloroplatinic acid ($\text{H}_2\text{Cl}_6\text{Pt} \cdot 6\text{H}_2\text{O}$) solution varied between 100, 500, and 1000 μL , which correspond to 0.32%, 1.6%, and 3.2% Pt, regarding the total weight of catalyst (wt%), respectively. The initial pH of the reaction was between 3.0 and 3.5.

Test of photolysis: The photodegradation of the phenol solution was also verified under UV light in the absence of the catalyst.

Test in the dark (adsorption): Phenol removal was also verified in the presence of catalyst but in the absence of UV light.

In all photocatalytic tests, the concentration of phenol was monitored by the colorimetric method (using 4-aminoantipyrine) [45,46], as this method quantifies the total phenolic compounds present in the solution. These measurements were carried out using a spectrophotometer; the calibration curve was read at $\lambda = 510 \text{ nm}$, and the removal % of phenol ($X\%$) was calculated by the following formula: $X (\%) = [(M_0 - M_f)/M_0] \times 100$, where M_0 and M_f mean the concentrations of phenol at the beginning and the final of each photocatalytic test, respectively.

3.3.1. Variation of pH of the Solution

To verify the influence of pH on the photocatalytic reaction, photocatalytic tests were carried out with phenol solution in different pH: pH 1.00, 3.5, 7.00, and 10.00, (at the beginning of the reaction). The percent of phenol removal of the photocatalytic process at a

natural pH (which means without pH modification) was also verified. Both the seawater and the phenol solution (40 ppm of phenol in seawater) had a pH of 8.4. In these tests, every test used 0.0125 g of catalyst, 25 mL of phenol solution, and 500 μL of platinum. The photocatalytic tests started for 20 min in the dark followed by 5 h under UV light.

3.3.2. Verification of Oxidizing Species

In order to describe the reaction mechanism that takes place over the catalyst, a set of experiments was carried out in the presence of scavengers of oxidant species. The following scavengers were used individually (at a concentration of 2 mM) in the photoreaction to quench a specific reactive species: ethanol (EtOH), p-benzoquinone (BQ), and potassium iodide (KI) to capture hydroxyl radicals ($\bullet\text{OH}$), anionic superoxide radicals ($\text{O}_2^{\bullet-}$) and positively charged holes (h^+), respectively. Each photocatalytic test of this experiment was performed in duplicate, with 500 μL platinum solution, 0.0125 g of catalyst, 25 mL of phenol solution, and 5 h of UV irradiation. The methodology was adapted from Rosli et al. [57].

3.3.3. Hydroxyl Radical Measurement Experiments ($\bullet\text{OH}$)

It is known that the reaction between terephthalic acid (TA) and $\bullet\text{OH}$ produces a highly fluorescent molecule, 2-hydroxyterephthalic acid (2-HTA), which shows a signal at a wavelength of 425 nm, making its detection feasible [57,58]. For this reason, for a better understanding of the formation of the hydroxyl radical ($\bullet\text{OH}$) during the photocatalytic degradation experiments, terephthalic acid (TA) was used as a proven molecule in the photocatalytic tests using the catalysts in the presence and the absence of Pt (1000 μL of platinum solution) in distilled water. The 2-HTA was detected with a fluorescence spectrophotometer (Shimadzu RF-5301, Kyoto, Japan) to monitor the fluorescence emission at a wavelength of 425 nm with excitation at 315 nm.

3.3.4. Catalyst Reuse

The photocatalysts were reused up to three times (in other words: three cycles). Each experiment was carried out under the following conditions: catalyst dosage of $0.5 \text{ g}_{\text{cat}} \cdot \text{L}^{-1}$, initial pH of the phenolic solution = 3.0–3.5, and three amounts of platinum (100, 500, and 1000 μL). The reaction time in the dark was 20 min, followed by 5 h under UV light. After each test, the samples were centrifuged, washed with clean (deionized) water three times, centrifuged, and finally dried at 130 $^\circ\text{C}$. Platinum was added only in the first cycle.

3.3.5. Comparison with Other Studies

One of the highlights of this paper is the treatment of effluent with high salinity, as there are few works in the area of heterogeneous photocatalysis for this application due to the difficulty caused by the high concentration of ions present in seawater. For comparative purposes, Table 3 shows the data reported in other works regarding the removal of phenol in the sea or distilled water, using different catalysts. According to this table, our material is competitive.

Table 3. Comparative data on phenol removal reported in other works.

Phenol Removal (%)	Phenol Initial Concentration (mg/L)	Application	Catalyst	Catalyst Concentration (g/L)	Degradation Time (h)	Reference
65	40	Seawater	(NaNbO ₃ /NaNb ₃ O ₈)/NiO + 3.2% Pt	0.5	5	This paper
60	50	Seawater	I/TiO ₂	0.5	3	Deng et al. [65]

Table 3. Cont.

Phenol Removal (%)	Phenol Initial Concentration (mg/L)	Application	Catalyst	Catalyst Concentration (g/L)	Degradation Time (h)	Reference
50	25	Seawater	La ³⁺ -doped Red-GO-TiO ₂	0.5	5	Wang et al. [66]
98	200	Seawater	TiO ₂ P25	0.5	25 * Hybrid process * 24 h activated sludge + 1 h Photocatalysis	L'Amour et al. [67]
76	15	distilled water	Ag-TiO ₂	0.2	2	Scott et al. [68]

4. Conclusions

This research reports a simple method to obtain a heterostructure material composed of niobates, according to the XRD, this material is composed of NaNbO₃/NaNb₃O₈/NiO.

The resultant material has a band gap energy equal to 3.12 eV and a surface area of 5.030 m²/g, similar to other materials usually used in heterogeneous photocatalysis.

The addition of a small amount of Pt⁰ on the heterostructure produced a photocatalyst with very good photocatalytic activity. This photocatalyst proved to be useful for the treatment of water-containing phenol with high salinity (seawater). The NiNb/Pt photocatalyst removed up to 65% of phenol in seawater in 5 h of reaction. This material can be applied in photocatalysis in a wide range of pH 1.00–8.5, and it can be reused several times.

The mechanism of photodegradation of phenol in seawater over the photocatalyst occurs preferentially by the generation of superoxide and hydroxyl radicals.

This research contributes to the development of new techniques for the treatment of saline effluents, as well as to the application of new materials based on niobium.

Author Contributions: Methodology, Y.J.O.A. and K.G.C.; validation, Y.J.O.A. and K.G.C.; formal analysis, Y.J.O.A. and K.G.C.; investigation, Y.J.O.A. and K.G.C.; resources, Y.J.O.A.; data curation, Y.J.O.A.; writing—original draft preparation, K.G.C.; writing—review and editing, K.G.C. and Y.J.O.A.; visualization, Y.J.O.A. and K.G.C.; supervision, Y.J.O.A.; project administration, Y.J.O.A. All authors have read and agreed to the published version of the manuscript.

Funding: The São Paulo Research Foundation (FAPESP) for the financial support (Grant N^o: 2014/24940-5), and the Brazilian National Council for Scientific Development (CNPq, Grant N^o 407097/20).

Data Availability Statement: Not applicable.

Acknowledgments: The authors thank the São Paulo Research Foundation (FAPESP) for the financial support (Grant N^o: 2014/24940-5), and the Brazilian National Council for Scientific Development (CNPq, Grant N^o 407097/20). And thanks to the Multiuser Experimental Center (CEM)—UFABC for the SEM analysis.

Conflicts of Interest: The authors declare no conflict of interest.

References

- MSDS—Chemical Product Safety Data Sheet—Phenol. Sigma-Aldrich. 2011. Available online: <https://sites.ffclrp.usp.br/cipa/fispq/Fenol.pdf> (accessed on 20 November 2022).
- Neff, J.M. *Bioaccumulation in Marine Organisms Effect of Contaminants From Oil Well Produced Water*; Elsevier Science: Amsterdam, The Netherlands, 2002; p. 468.
- Motta, A.R.P.; Borges, C.P.; Kiperstok, A.; Esquerre, K.P.; Araujo, P.M. Produced water treatment for oil removal by membrane separation process: Review. *Eng. Sanit. Ambient* **2013**, *18*, 15–26. [CrossRef]
- ANP- Monthly Bulletin of Oil and Natural Gas Production. The National Agency of Petroleum, Natural Gas and Biofuels. 2021. Available online: <https://www.gov.br/anp/pt-br/centrais-de-conteudo/publicacoes/bulletins-anp/bulletin-mensal-da-producao-de-petroleo-e-gas-natural> (accessed on 20 November 2022).

5. Jing, S.; Li, T.; Li, X.; Xu, Q.; Hu, J.; Li, R. Phenolic foams modified by cardanol through bisphenol modification. *J. Appl. Polym. Sci.* **2014**, *131*, 39942. [[CrossRef](#)]
6. Lei, P.; Wang, F.; Gao, X.; Ding, Y.; Zhang, S.; Zhao, J.; Liu, S.; Yang, M. Immobilization of TiO₂ nanoparticles in polymeric substrates by chemical bonding for multi-cycle photodegradation of organic pollutants. *J. Hazard. Mater.* **2012**, *227–228*, 185–194. [[CrossRef](#)] [[PubMed](#)]
7. Bessa, E.; Santanna, J.; Dezotti, M. Photocatalytic/H₂O₂ treatment of oil field produced waters. *Appl. Catal. B Environ.* **2001**, *29*, 125–134. [[CrossRef](#)]
8. Braga, U. Use of Clay Minerals and Diatomite as an Adsorbent for Phenols in Water Produced in the Oil Industry. Master's Thesis, Universidade Federal do Rio Grande do Norte, Natal, Brazil, 2018. Available online: <https://repositorio.ufrn.br/handle/123456789/12884> (accessed on 20 November 2022).
9. Asencios, Y.; Lourenço, V.; Carvalho, W. Removal of phenol in seawater by heterogeneous photocatalysis using activated carbon materials modified with TiO₂. *Catal. Today* **2022**, *388–389*, 247–258. [[CrossRef](#)]
10. Chamara, L.S.; Ravinder, K.; Garlapalli, J.P.T.; Trembly, J.P. Removal of phenol from oil/gas produced water using supercritical water treatment with TiO₂ supported MnO₂ catalyst. *J. Environ. Chem. Eng.* **2017**, *5*, 488–493.
11. CONAMA—National Environment Council of Brazil. Resolution N^o. 430, 05/13/2011. Available online: <https://www.braziliannr.com/brazilian-environmental-legislation/conama-resolution-43011/> (accessed on 20 November 2022).
12. Asencios, Y.J.O.; Quijo, V.; Francielle, M.; Nogueira, A.; Rocca, R.; Assaf, E.M. Photocatalytic activity of Nb heterostructure (NaNbO₃/Na₂Nb₄O₁₁) and Nb/clay materials in the degradation of organic compounds. *Solar Energy* **2019**, *194*, 37–46. [[CrossRef](#)]
13. Choi, J. Development of Visible- Light-Active Photocatalyst for Hydrogen Production and Environmental Application. Ph.D. Thesis, California Institute of Technology, Pasadena, CA, USA, 2010.
14. Ibhaddon, A.; Fitzpatrick, P. Heterogeneous photocatalysis: Recent advances and applications. *Catalysts* **2013**, *3*, 189–218. [[CrossRef](#)]
15. Kim, J.; Choi, W. Hydrogen producing water treatment through solar photocatalysis. *Energy Environ. Sci.* **2010**, *3*, 1042–1045. [[CrossRef](#)]
16. Ferraz, N.P.; Marcos, C.F.; Nogueira, A.E.; Martins, A.S.; Assaf, E.M.; Asencios, Y.J.O. Hexagonal-Nb₂O₅/Anatase-TiO₂ mixtures and their applications in the removal of Methylene Blue dye under various conditions. *Mater. Chem. Phys.* **2017**, *198*, 331–340. [[CrossRef](#)]
17. Yang, F.; Zhang, Q.; Zhang, L.; Liu, Q.; Dai, W. Facile synthesis of highly efficient Pt/N-rGO/N-NaNbO₃ nanorods toward photocatalytic hydrogen production. *Appl. Catal. B Environ.* **2019**, *257*, 117901. [[CrossRef](#)]
18. Agostini, G.; Lamberti, C. *Characterization of Semiconductor Heterostructures and Nanostructures*; Elsevier: Amsterdam, The Netherlands, 2011.
19. Fan, M.; Hu, B.; Yan, X.; Song, C.; Chen, T.; Feng, Y.; Shi, W. Excellent visible-light driven photocatalytic performance of Cu₂O sensitized NaNbO₃ heterostructures. *New J. Chem.* **2015**, *39*, 6171–6177. [[CrossRef](#)]
20. Li, G.; Wang, W.; Yang, N.; Zhang, W.F. Composition dependence of AgSbO₃/NaNbO₃ composite on surface photovoltaic and visible-light photocatalytic properties. *App. Phys. A* **2011**, *103*, 251–256. [[CrossRef](#)]
21. Kumar, S.; Khanchandani, S.; Thirumal, M.; Ganguli, A.K. Achieving enhanced visible-light-driven photocatalysis using type-II NaNbO₃/CdS core/shell heterostructures. *ACS Appl. Mater. Interf.* **2014**, *6*, 13221–13233. [[CrossRef](#)]
22. Zhou, W.; Yao, M.; Guo, L.; Li, Y.; Li, J.; Yang, S. Hydrazine-Linked Convergent Self-Assembly of Sophisticated Concave Polyhedrons of β-Ni(OH)₂ and NiO from Nanoplate Building Blocks. *J. Am. Chem. Soc.* **2009**, *131*, 2959. [[CrossRef](#)]
23. Joshi, M.; Labhsetwar, K.; Parwate, D.V. Efficient photocatalytic hydrogen generation by silica supported and platinum promoted titanium dioxide. *Mater. Res. Bull.* **2013**, *48*, 3545–3552. [[CrossRef](#)]
24. Silva, P.C.; Ferraz, N.P.; Perpetuo, E.A.; Asencios, Y.J.O. Oil produced water treatment using advanced oxidative processes: Heterogeneous-photocatalysis and photofenton. *J. Sediment. Environ.* **2019**, *4*, 99–107. [[CrossRef](#)]
25. Wang, T.; Li, B.R.; Pan, J.H.; Wu, L.G.; Wang, Z.Q.; Wang, Z.H.; Jiang, B.Q. Deposition of quantum-sized Ag on TiO₂ through adsorbed-layer nanoreactor synthesis and its performance for photodegrading phenol in seawater under visible-light irradiation. *Colloids Surfaces A Physicochem. Eng. Asp.* **2018**, *555*, 448–456. [[CrossRef](#)]
26. George, R.T.; Dar, T.A.; Joshi, D.C.; Sathe, V.; Rathore, A.K.; Thota, S. Thermal hysteresis and vibrational excitations in NiO containing NaNbO₃. *J. Phys. D Appl. Phys.* **2019**, *52*, 115301. [[CrossRef](#)]
27. George, R.T.; Joshi, D.C.; Nayak, S.; Tiwari, N.; Chauhan, R.N.; Pramanik, P.; Dar, T.A.; Ghosh, S.; Thota, S. Effect of NiO substitution on the structural and dielectric behavior of NaNbO₃. *J. Appl. Phys.* **2018**, *123*, 054101. [[CrossRef](#)]
28. Zielińska, B.; Borowiak-Palen, E.; Kalenczuk, R.J. Preparation, characterization and photocatalytic activity of metal-loaded NaNbO₃. *J. Phys. Chem. Solids* **2011**, *72*, 117–123. [[CrossRef](#)]
29. Iwase, A.; Saito, K.; Kudo, A. Sensitization of NaMO₃ (M: Nb and Ta) Photocatalysts with Wide Band Gaps to Visible Light by Ir Doping. *Bull. Chem. Soc. Jpn.* **2011**, *82*, 514–518. [[CrossRef](#)]
30. Kioka, K.; Honma, T.; Oh-ishi, K.; Reibstein, S.; Da, N.; Wondraczek, L.; Komatsu, T. Effect of Al₂O₃ addition on the formation of perovskite-type NaNbO₃ nanocrystals in silicate-based glasses. *J. Non-Cryst. Solids* **2012**, *358*, 1523–1529. [[CrossRef](#)]
31. Anastas, P.T.; Warner, J.C. *Green Chemistry: Theory and Practice*; Oxford University Press: New York, NY, USA, 1998; p. 30.
32. Souza, J.K.D. Photocatalytic Evaluation of Lamellar Niobates: Influence of Synthesis Methods, Theoretical and Experimental Aspects. Ph.D. Thesis, Universidade Federal da Paraíba, Paraíba, Brazil, 2018. Available online: <https://repositorio.ufpb.br/jspui/handle/123456789/14841> (accessed on 20 November 2022).

33. Bhatkhande, D.S.; Kamble, S.P.; Sawant, S.B.; Pangarkar, V.G. Photocatalytic and photochemical degradation of nitrobenzene using artificial ultraviolet light. *Chem. Eng. J.* **2004**, *102*, 283–290. [CrossRef]
34. Almeida, T.P.; Fay, M.W.; Hansen, T.W.; Zhu, Y.; Brown, P.D. Insights from in situ and environmental TEM on the oriented attachment of α -Fe₂O₃ nanoparticles during α -Fe₂O₃ nanorod formation. *Cryst. Eng. Comm.* **2014**, *16*, 1540–1546. [CrossRef]
35. Lourenço, V.S.; Boto, S.M.; Carvalho, W.A.; Asencios, Y.J. Peruíbe black mud based catalysts for the removal of organic pollutants in water. *J. Sediment. Environ.* **2020**, *5*, 293–305. [CrossRef]
36. Pinheiro, N.D.A. Lamellar Niobates (KNb₃O₈ and K₄Nb₆O₁₇) Synthesized by the Polymeric Precursor Method and Applied in the Photodegradation of the Remazol Yellow Gold Dye. Master's Thesis, Universidade Federal da Paraíba, Paraíba, Brazil, 2020. Available online: <https://repositorio.ufpb.br/jspui/handle/123456789/18196> (accessed on 20 November 2022).
37. Praxedes, F.R. Sodium and Potassium Niobates Obtained by the Spray Pyrolysis Method: Characterization and Photocatalytic Activity for the Decolorization of Aqueous Solutions of Dyes. Master's Thesis, Universidade Estadual Paulista, São Paulo, Brazil, 2019. Available online: <https://repositorio.unesp.br/handle/11449/181471> (accessed on 20 November 2022).
38. Ferreira, I.V.L.; Daniel, L.A. Heterogeneous photocatalysis with TiO₂ applied to the treatment of secondary sanitary sewage. *Eng. Sanit. Ambient.* **2004**, *9*, 335–342. [CrossRef]
39. Salgado, J.R.C.; Gonzalez, E.R. Correlation between catalytic activity and particle size of Pt/C prepared by different methods. *Eclat. Quím.* Online. **2003**, *28*, 77–85. [CrossRef]
40. Ghorai, T.K.; Dhak, P. Niobium Oxides: An overview of the synthesis of Nb₂O₅ and its application in Heterogeneous Photocatalysis. *Adv. Mater. Lett.* **2013**, *4*, 121–130.
41. Assis, R.B. Synthesis of Sodium and Potassium Niobate (K_{1-x}NaxNbO₃) with Photocatalytic and Photoluminescent Properties. Ph.D. Thesis, Federal University of Rio Grande do Norte, Natal, Brazil, 2017. Available online: <https://repositorio.ufrn.br/handle/123456789/45428> (accessed on 20 November 2022).
42. Wu, J.; Xue, D. Advances in Chemical Synthesis of Nb-Containing Oxides. *J. Nanoeng. Nanomanuf.* **2011**, *2*, 136–154. [CrossRef]
43. Shishido, T.; Miyatake, T.; Teramura, K.; Hitomi, Y.; Yamashita, H.; Tanaka, T. Mechanism of photooxidation of alcohol over Nb₂O₅. *J. Phys. Chem. C* **2009**, *113*, 18713–18718. [CrossRef]
44. Gonçalves, M.C.P.; Padilha, S.R.R.; Lopes, M.F.; Paris, E.C. Application of commercial Nb₂O₅ for decolorization of methylene blue dye by photocatalysis process. *Rev. Eng. Tecnol.* **2017**, *9*, 95–105. Available online: <https://revistas.uepg.br/index.php/ret/article/view/11269> (accessed on 20 November 2022).
45. APHA. *Standard Methods for the Examination of Water and Wastewater*, 17th ed.; American Public Health Association: Washington, DC, USA, 1989.
46. EPA (US Environmental Protection Agency). *Method 604, Methods for Organic Chemical Analysis of Municipal and Industrial Wastewater*; Part VIII, 40 CFR Part 136. Appendix A; Environmental Protection Agency EPA: Washington, DC, USA, 1984.
47. Ziolli, W.; Jardim, F. Photocatalytic decomposition of seawater-soluble crude-oil fractions using high surface area colloid nanoparticles of TiO₂. *J. Photochem. Photobiol. A Chem.* **2002**, *147*, 205–212. [CrossRef]
48. Shaban, Y.A.; El Sayed, M.A.; El Maradny, A.A.; Al Farawati, R.K.; Al Zobidi, M.I. Photocatalytic degradation of phenol in natural seawater using visible light active carbon modified (CM)-n-TiO₂ nanoparticles under UV light and natural sunlight illuminations. *Chemosphere* **2013**, *91*, 307–313. [CrossRef]
49. Hippargi, G.; Mangrulkar, P.; Chilkalwar, A.; Labhsetwar, N.; Rayalu, S. Chloride ion: A promising hole scavenger for photocatalytic hydrogen generation. *Int. J. Hydrogen Energy* **2018**, *43*, 6815–6823. [CrossRef]
50. Asencios, Y.J.; Machado, V.A. Photodegradation of Organic Pollutants in Seawater and Hydrogen Production via Methanol Photoreforming with Hydrated Niobium Pentoxide Catalysts. *Sustain. Chem.* **2022**, *3*, 172–191. [CrossRef]
51. Iguchi, S.; Teramura, K.; Hosokawa, S.; Tanaka, T. Effect of chloride ion as a hole scavenger on the photocatalytic conversion of CO₂ in an aqueous solution over Ni–Al layered double hydroxides. *Phys. Chem.* **2015**, *17*, 17995–18003. [CrossRef]
52. Kinney, L.C.; Ivanuski, V.R. *Photolysis Mechanisms for Pollution Abatement*, Available on U.S. Department of the Interior; Federal Water Pollution Control Administration: Cincinnati, OH, USA, 1969.
53. Beker, U.; Ganbold, B.; Dertli, H.; Gülbayir, D.D. Adsorption of phenol by activated carbon: Influence of activation methods and solution pH. *Energy Convers. Manag.* **2010**, *51*, 235–240. [CrossRef]
54. Lopes, W.S.; Azevedo, M.G.; Leite, V.D.; Sousa, J.T.; Buriti, J.S. Degradation of 17 α -ethinylestradiol in water by heterogeneous photocatalysis. *Rev. Ambient. Água.* **2015**, *10*, 728–736. [CrossRef]
55. Lam, S.M.; Sin, J.C.; Satoshi, I.; Abdullah, A.Z.; Mohamed, A.R. Enhanced sunlight photocatalytic performance over Nb₂O₅/ZnO nanorod composites and the mechanism study. *Appl. Catal. A Gen.* **2014**, *471*, 126–135. [CrossRef]
56. Ji, P.; Zhang, J.; Chen, F.; Anpo, M. Study of adsorption and degradation of acid orange 7 on the surface of CeO₂ under visible light irradiation. *Appl. Catal. B Environ.* **2009**, *85*, 148–154. [CrossRef]
57. Rosli, M.; Lam, N.I.; Sin, S.M.; Satoshi, J.C.; Mohamed, A.R. Photocatalytic Performance of ZnO/gC₃N₄ for Removal of Phenol under Simulated Sunlight Irradiation. *J. Environ. Eng.* **2018**, *144*, 04017091. [CrossRef]
58. Tong, T.; Zhang, H.; Chen, J.; Jin, D.; Cheng, J. The photocatalysis of BiFeO₃ disks under visible light irradiation. *Catal. Commun.* **2016**, *87*, 23–26. [CrossRef]
59. Yao, S.; Li, J.; Shi, Z. Immobilization of TiO₂ nanoparticles on activated carbon fiber and its photodegradation performance for organic pollutants. *Particuology* **2010**, *8*, 272–278. [CrossRef]

60. Buxton, G.V.; Greenstock, C.L.; Helman, W.P.; Ross, A.B. Critical review of rate constants for reactions of hydrated electrons, hydrogen atoms and hydroxyl radicals (OH/O⁻) in aqueous solution. *J. Phys. Chem. Ref. Data* **1988**, *17*, 513–886. [[CrossRef](#)]
61. Haque, M.M.; Muneer, M. Photodegradation of norfloxacin in aqueous suspensions of titanium dioxide. *J. Hazard. Mater.* **2007**, *145*, 51–57. [[CrossRef](#)]
62. Carvalho, K.T.G.; Silva, A.C.; Oliveira, L.C.A.; Goncalves, M.; Magriotis, Z.M. Modified synthetic niobia as catalyst in the oxidation of organic dye: Utilization of H₂O₂ and atmospheric O₂ as oxidants. *Química Nova* **2009**, *32*, 1373–1377. [[CrossRef](#)]
63. Nogueira, A.E.; Oliveira, L.C.; Ramalho, T.C. Photocatalytic degradation of organic compound in water using synthetic niobia: Experimental and theoretical studies. *Top. Catal.* **2011**, *54*, 270–276. [[CrossRef](#)]
64. Wood, D.L.; Tauc, J. Weak Absorption Tails in Amorphous Semiconductors. *Phys. Rev. B.* **1972**, *5*, 3144–3151. [[CrossRef](#)]
65. Deng, P.C.; Hu, J.Z.; Wang, H.Z. Photodegradation of Phenol on Halogen-Doping TiO₂ Nanoparticles Composites in Seawater. *Mater. Sci. Forum* **2011**, *694*, 355–359.
66. Wang, T.; Xu, Z.Y.; Wu, L.G.; Li, B.R.; Chen, M.X.; Xue, S.Y.; Zhu, Y.C.; Cai, J. Enhanced photocatalytic activity for degrading phenol in seawater by TiO₂-based catalysts under weak light irradiation. *RSC Adv.* **2017**, *7*, 31921–31929. [[CrossRef](#)]
67. L'Amour, R.J.A.; Azevedo, E.B.; Leite, S.G.F.; Dezotti, M. Removal of phenol in high salinity media by a hybrid process (activated sludge + photocatalysis). *Sep. Purif. Technol.* **2008**, *60*, 142–146.
68. Scott, T.; Zhao, H.; Deng, W.; Feng, X.; Li, Y. Photocatalytic degradation of phenol in water under simulated sunlight by an ultrathin MgO coated Ag/TiO₂ nanocomposite. *Chemosphere* **2019**, *216*, 1–8. [[CrossRef](#)]